# *Visualization of microscale particle focusing in diluted and whole blood using particle trajectory analysis*



**Citation:** Lim, Eugene J. et al. "Visualization of Microscale Particle Focusing in Diluted and Whole Blood Using Particle Trajectory Analysis." Lab on a Chip 12.12 (2012): 2199.

**As Published:** http://dx.doi.org/10.1039/c2lc21100a

**Publisher:** Royal Society of Chemistry, The

**Persistent URL:** http://hdl.handle.net/1721.1/79094

**Version:** Author's final manuscript: final author's manuscript post peer review, without publisher's formatting or copy editing

# Visualization of microscale particle focusing in diluted and whole blood using particle trajectory analysis

**Eugene J. Lim[ab], Thomas J. Ober[c], Jon F. Edd[d], Gareth H. McKinley[c] and Mehmet Toner[b]**

[a]*Electrical Engineering and Computer Science Department, Massachusetts Institute of Technology, Cambridge, MA 02139*
[b]*Center for Engineering in Medicine and Surgical Services, Massachusetts General Hospital, Harvard Medical School, Charlestown, MA 02129*
[c]*Mechanical Engineering Department, Massachusetts Institute of Technology, Cambridge, MA 02139*
[d]*Mechanical Engineering Department, Vanderbilt University, Nashville, TN 37212*

## Abstract

Inertial microfluidics has demonstrated the potential to provide a rich range of capabilities to manipulate biological fluids and particles to address various challenges in biomedical science and clinical medicine. Various microchannel geometries have been used to study the inertial focusing behavior of particles suspended in simple buffer solutions or in highly diluted blood. One aspect of inertial focusing that is not studied is how particles suspended in whole or minimally diluted blood respond to inertial forces in microchannels. The utility of imaging techniques (i.e., high-speed bright-field imaging and long exposure fluorescence (streak) imaging) primarily used to observe particle focusing in microchannels is limited in complex fluids such as whole blood due to interference from large numbers of red blood cells (RBCs). In this study, we used particle trajectory analysis (PTA) to observe the inertial focusing behavior of polystyrene beads, white blood cells, and PC-3 prostate cancer cells in physiological saline and blood. Identification of in-focus (fluorescently labeled) particles was achieved at mean particle velocities of up to 1.85 m/s. Quantitative measurements of in-focus particles were used to construct intensity maps of particle frequency in the channel cross-section and scatter plots of particle centroid coordinates vs. particle diameter. PC-3 cells spiked into whole blood (*HCT* = 45%) demonstrated a novel focusing mode not observed in physiological saline or

diluted blood. PTA can be used as an experimental frame of reference for understanding the physical basis of inertial lift forces in whole blood and discover inertial focusing modes that can be used to enable particle separation in whole blood.

## Introduction

Inertial focusing of particles in microchannels have demonstrated potentially useful effects for a wide range of applications in basic science and clinical medicine,[1] including flow cytometry[2,3] and particle enrichment.[4-7] Fluid flow in microchannels has often been assumed to be governed by viscous forces based on the notion that small length scales require a correspondingly small Reynolds number. Particle migration across streamlines on the microscale was observed in straight square channels, in which randomly distributed particles focus to four positions centered along each face of the channel.[8-11] As the aspect ratio of the channel increases (i.e., a very wide or very tall channel), particle focusing reduces to predominantly two equilibrium positions centered at the long face of the channel.[12,13] Inertial lift forces induce lateral migration of particles to distinct equilibrium positions at finite particle Reynolds number, $R_p = R_c(aD_h^{-1})^2$, where $R_c$ is the channel Reynolds number, a is the particle diameter, and $D_h$ is the hydraulic diameter of the channel, defined as $D_h = 2wh(w+h)^{-1}$, where w and h are the channel width and height. Numerical modeling and direct experiments of size-varying particles flowing through straight square channels have yielded scaling of inertial lift force $F_L$.[12] The inertial lift force on a particle near the channel centerline scaled as $F_L \alpha \rho U^2 a^3 H^{-1}$, while $F_L \alpha \rho U^2 a^6 H^{-4}$ near the channel wall, where $\rho$ is the fluid density, $U$ is the mean flow velocity, $a$ is the particle diameter, and $H$ is the channel dimension. The spatial variation in how the force scales along the width dimension suggests the formation of equilibrium positions from two disparate fluid dynamic effects: 1) a “wall effect” lift that acts away from the wall

towards the channel centerline, and 2) a “particle shear” lift that acts down the gradient in the shear rate of the flow.[14,15]

One aspect of inertial focusing that is not studied is how particles suspended in complex fluids such as whole or minimally diluted blood respond to inertial forces in microchannels. Particle focusing in whole or minimally diluted blood has not been studied or utilized due to performance limitations in the imaging techniques (e.g., high-speed brightfield imaging and long exposure fluorescence (streak) imaging) commonly used to observe particle focusing. In high-speed bright-field imaging, individual particles imaged at resolution speeds exceeding $10^5$ frames per second using shutter speeds down to 1 μs has been used to measure size, rotation rate, and/or interparticle spacing of individual channels flowing through the channel.[4,12,16] In long exposure fluorescence imaging, the signal intensity of fluorescently labeled particles accumulated over a time interval on the order of 1 s has been used to measure mean equilibrium position, full width at half maximum, and/or separation efficiency of multiple particles flowing through the channel.[3,11,17] Both of these imaging techniques have been used to characterize particle focusing in starting samples consisting of physiological saline or highly diluted blood.[2,4,5] The utility of these imaging techniques becomes limited in starting samples consisting of whole or minimally diluted blood. In 1 ml of whole blood, there are approximately 5 x $10^9$ RBCs, 5 x $10^6$ WBCs, and 3 x $10^8$ platelets suspended in plasma. High-speed bright-field imaging is limited by the overwhelming presence of RBCs obscuring vision of individual particles in the channel, while long-exposure fluorescence imaging is limited by attenuation of incident light by hemoglobin absorption and RBC light scattering in the visible region. For both imaging techniques, it is difficult to gather information in the y-axis (i.e., along the height dimension of the channel).

*In vitro* studies of blood flow through capillary tubes have shown that blood behaves as a Newtonian fluid for tube diameters larger than 500 μm, and as a non-Newtonian fluid for tube diameters smaller than 500 μm. This non-Newtonian behavior, known as the Fahraeus-

Lindqvist effect, is marked by a decrease in apparent blood viscosity for smaller tube diameters.[18] This is due to the formation of a cell-free layer near the tube wall that has a lower viscosity relative to the RBC-rich tube core[19,20]. Initial studies on the behavior of RBCs in shear flow were primarily limited to dilute blood suspensions due to the lack of imaging techniques capable of obtaining both direct and quantitative measurements of multiple RBC motions in concentrated blood suspensions. Visualization and detection of tracer RBCs at $HCT > 10\%$ was first achieved using ghost cells (i.e., ruptured RBCs that were resealed in the absence of hemoglobin) and a traveling microscope for channel Reynolds numbers $R_c = U_m D_h / v = 0.3$, where $U_m$ is the maximum channel velocity, $D_h$ is the hydraulic diameter, and $v$ is the kinematic viscosity.[21] Ghost cells were used as models of RBCs due to attenuation of incident light by hemoglobin absorption and RBC light scattering when measuring high concentrations of normal RBCs.

The development of spinning disk (Nipkow) confocal microscopy used with laser illumination made it possible to generate a sufficient signal-to-noise ratio for detecting RBC motion for $HCT > 10\%$.[22] Recent work utilized fluorescent dye labeling, scanning confocal microscopy, and micro-particle image velocimetry (μPIV) to observe near-wall RBC motion at physiologic high-hematocrit (i.e., $HCT = 48\%$) blood in a rectangular microchannel for $R_c = 0.03$.[23] The intensity of Nd:YAG (or comparable) laser illumination is such that only brief pulses (~ 10 ns) of light are needed to detect fluorescently labeled particles found in its path. Such an imaging technique could be used to identify various properties (e.g., three-dimensional position, particle diameter, rotation rate) of individual particles in whole blood flowing through the channel at high $R_p$. These experimental measurements can be used to make quantitative measurements of particle focusing behavior in whole blood. Moreover, an experimental frame of reference can be provided for *in silico* studies of RBC (and other particle) motion in blood that account for both the deformability of an individual RBC and the cell-cell interactions from a large number of RBCs. In particular, it may be possible to provide a physical basis of particle

focusing in blood using computational models that quantitatively predict the rheological properties and dynamics of blood flow.[24,25]

In this study, particle tracking analysis (PTA) was used to characterize the effect of RBCs on particle motion in inertia-dominated flow. Fluorescently labeled particles were suspended in physiological saline, diluted blood, or whole blood prior to being processed in a straight rectangular channel with a 2:1 aspect ratio. Images taken at multiple vertical positions in the channel were used to find in-focus particles and determine their particle diameter and two-dimensional spatial coordinates within the channel cross-section. The inertial focusing behavior of polystyrene beads, WBCs, and PC-3 human prostate cancer cell lines was characterized as a function of flow rate $Q$ and RBC volume fraction $f_{RBC}$. Rheometer measurements of blood viscosity and shear rate were used to provide insight into PTA measurements of PC-3 cell focusing behavior in diluted and whole blood.

## Materials and methods

### Device fabrication

A straight rectangular channel (h = 93 μm, w = 45 μm, L = 3.5 cm) was formed in polydimethylsiloxane (PDMS) using a master mold fabricated via photolithography.[26] A 4-inch silicon wafer was spin-coated with a 93 μm thick layer of negative photoresist (SU-8 100, Microchem, Newton, MA), exposed to UV-light through a Mylar photomask (Fineline Imaging Colorado Springs, CO), and developed (BTS-220, J.T. Baker, Phillipsburg, NJ). A 10:1 mix of PDMS elastomer and curing agent (Sylgard 184, Dow Corning, Midland, MI) were poured onto the master mold and degassed for 60 min to remove all trapped bubbles. The master mold was placed in a 80°C oven for 72 h to thoroughly cure the PDMS. The cured PDMS replica was peeled away from the master mold before inlet, outlet, and height calibration holes were punched using a coring tool (Harris Uni-Core, Redding, CA) with a hole diameter of 1.5 mm.

The hole punched PDMS replica was irreversibly bonded to a glass coverslip by exposing both PDMS and glass surfaces to $O_2$ plasma (Harrick Plasma, Ithaca, NY).

**Particle suspensions**

Fluorescently labeled polystyrene beads (FluoSpheres, Invitrogen, Carlsbad, CA) were supplied as stock suspensions in 0.15M NaCl with 0.05% Tween 20 and 0.02% thimerosal. PC-3 human prostate cancer cells (CRL-1435, ATCC) were grown in F-12K medium (30-2004, ATCC, Manassas, VA) containing 10% fetal bovine serum (Invitrogen, Carlsbad, CA) and 1% penicillin streptomycin (Invitrogen, Carlsbad, CA) at 37°C under 5% $CO_2$ conditions. PC-3 cells were fluorescently labeled in physiological saline (Invitrogen, Carlsbad, CA) containing 5 μM calcein red-orange AM (Invitrogen, Carlsbad, CA). Whole blood samples from healthy donors were obtained (Research Blood Components, Boston, MA) in venous blood collection tubes containing EDTA (Vacutainer, BD Biosciences, San Jose, CA). The RBC volume fraction (i.e., hematocrit count) in each sample was determined using a blood analyzer (KX-21, Sysmex, Mundelein, IL). WBCs were recovered from whole blood via RBC lysis buffer (Miltenyi Biotec, Auburn, CA) and fluorescently labeled in physiological saline containing 5 μM calcein red-orange AM. Samples with a specific RBC volume fraction were generated by suspending particles in appropriate amounts of physiological saline and whole blood. The particle concentration was set at $3.0 \times 10^6$ particles/ml.

**μPIV image capture of fluorescently labeled particles**

The starting sample containing fluorescently labeled particles was injected into the microchannel using an automated syringe pump (PhD 2000, Harvard Apparatus, Holliston, MA) at flow rates of Q = 50, 150, and 450 μl/min. This corresponds to particle velocities of U = 0.21, 0.62, and 1.85 m/s. The sample loading system consisted of 5-ml syringe (BD Biosciences, San Jose, CA), 22-gauge blunt needle (Small Parts, Seattle, WA), 0.02-inch inner diameter

tubing (Tygon, Small Parts, Seattle, WA), and cyanoacrylate adhesive (Loctite, Henkel, Rocky Hill, CT). Images of particles flowing through the channel were captured using Nd:YAG laser-light illumination (LaVision, Ypsilanti, MI), an epi-fluorescent inverted microscope (TE-2000, Nikon, Melville, NY), and a charge-coupled device camera (TSI, Shoreview, MN). The laser generated 10-ns pulses of light with an excitation wavelength of 532 nm, and the camera detected light from fluorescent particles with an emission wavelength exceeding 565 nm. At a stationary location 3.5 cm downstream from the channel entrance, images were captured at 8 different height positions spaced 6 μm apart. Prior to image capture, 2 μm polystyrene beads (FluoSpheres, Invitrogen, Carlsbad, CA) were placed in open wells formed when one side of the height calibration holes in the PDMS replica was bonded to a glass coverslip. In-focus polystyrene beads found at the bottom of the well were used to establish the zero height position (i.e., floor) of the channel. For each height position, a set of 400 images were collected at a rate of 5 frames per second.

**μPIV image analysis of fluorescently labeled particles**

ImageJ software (NIH, Bethesda, MD) was used to process raw images and identify in-focus particles at each height position. For an in-focus particle at a given height location, images were taken at multiple height positions in order to observe corresponding changes in fluorescence signal intensity indicative of an out-of-focus particle. An in-focus particle was predominantly found to exhibit both a higher mean 8-bit grayscale value and a steeper edge signal intensity gradient relative to an out-of-focus particle. For each set of 400 images at a given height location, an image threshold was automatically set using an iterative procedure based on the isodata algorithm.[27] Using a specific cutoff for particle size based on size distribution measurements from a cell analyzer, the image filtering technique automatically generated a table of potential in-focus particles. All particles were marked in the set of images and referenced numerically in the table, and each particle was characterized based on a user-

defined set of parameters (e.g., 2-D particle area, mean signal intensity, x-y coordinates, and circularity). The collection of potential in-focus particles were examined manually to ensure that in-focus particles were identified and measured properly. For a given flow rate and RBC volume fraction, quantitative measurements from the collection of in-focus particles were used to construct surface and scatter plots characterizing various aspects of particle focusing behavior in MATLAB (Mathworks, Natick, MA).

## Results

### Image capture of individual in-focus particles in diluted blood

Particle trajectory analysis (PTA) was used to identify polystyrene beads, white blood cells, and PC-3 cells over a range of flow rates $Q$ and RBC volume fractions $f_{RBC}$, where $f_{RBC}$ is the ratio of RBC volume to the starting sample volume. For example, $HCT$ = 45% (i.e., whole blood in this study) corresponds to $f_{RBC}$ = 1, while $HCT$ = 15% corresponds to $f_{RBC}$ = 0.33 (diluted using physiological saline). A straight rectangular channel with a 2:1 (h/w) aspect ratio was used to focus randomly distributed particles to two lateral equilibrium positions centered on the long face of the channel (Fig. 1a). These equilibrium positions resulted from a balance of a "wall effect" lift that acts away from the wall towards the channel centerline and a "particle shear" lift that acts away from the channel centerline towards the wall (Fig. 1b). Polystyrene beads (mean particle diameter $a_m$ = 9.9 μm) used in this study were monodisperse in nature, while white blood cells ($a_m$ = 9.0 μm, size range of 7-11 μm) and PC-3 cells ($a_m$ = 17.8 μm, size range of 10-35 μm) were polydisperse in nature. Given a 20x objective with a numerical aperture of 0.4, the depth of field was calculated[28] to be $\delta_y$ = 5.8 μm. In order to reliably differentiate between in-focus particles found at neighboring vertical positions, the spacing between all vertical positions was set to 6 μm. The imaging locations were confined to the

bottom half of the channel since particle focusing was expected to be symmetric across the *x*-*z* plane at $y$ = 48 μm.

In diluted blood samples where the utility of high-speed bright-field imaging and long-exposure fluorescence is limited, PTA demonstrated the ability to capture images of individual in-focus particles moving at ultra-fast velocities (Fig. S1). Image capture of individual in-focus particles (with no evidence of particle streaks) was achieved at flow rates up to $Q$ = 450 μl/min in physiological saline initially, which corresponds to a mean flow velocity of $U$ = 1.85 m/s and a channel Reynolds number of $R_c$ = 158. We limited our study to this range of flow rates, as flow rates beyond $Q$ = 450 μl/min for $f_{RBC}$ = 1 generated a fluid pressure at the device inlet that exceeded the critical de-bonding pressure of the PDMS-glass interface. At a given vertical position (e.g., $y$ = 48 μm), in-focus particles exhibited peak and uniform fluorescence signal intensity, while out-of-focus particles exhibited sub-optimal and radially diffuse fluorescence signal intensity (Fig. 1c). Using the appropriate image threshold, it was possible to differentiate in-focus particles at a given vertical position from in-focus particles at neighboring vertical positions. As a result, in-focus particles found at all vertical positions were used to make quantitative measurements of particle focusing behavior. Once PTA-based identification of individual in-focus particles was established in physiological saline, we repeated these experiments for polystyrene beads, white blood cells, and PC-3 prostate cancer cells suspended in diluted blood (Fig. 1d). As $f_{RBC}$ increased, in-focus particles exhibited a fluorescence signal intensity that was weaker and less uniform. However, it was still possible to distinguish likely in-focus particles from undoubtedly out-of-focus particles for a given $Q$ and $f_{RBC}$.

**Quantitative measurements of particle focusing behavior in diluted blood**

For a given $Q$ and $f_{RBC}$, in-focus particles from all vertical positions were used to make quantitative measurements of particle focusing behavior. The distribution of particles in the

channel cross-section (*y*-*z* plane) was visualized using an intensity map in which each individual rectangle represented a possible location for the centroid ($y_c$, $z_c$) of an in-focus particle. The color scale used to represent the particle frequency $n_f$ at a given point in the *y*-*z* plane consisted of full color (for $n_f > 10$), grayscale (for $1 < n_f < 10$), and white (for $n_f = 0$). Given the polydisperse nature of white blood cells and PC-3 cells, a scatter plot of lateral centroid coordinate $z_c$ vs. particle diameter *a* was constructed. For a straight rectangular channel with a 2:1 (h/w) aspect ratio, particle focusing is predominantly reduced to two lateral equilibrium positions centered on the long face. Particle focusing to lateral equilibrium positions have been shown to occur both at a single vertical position[8] and over a wide range of vertical positions[29]. Applications in flow cytometry would require the former, while applications in rare cell isolation can utilize the latter provided that particle focusing achieves the desired particle separation benchmarks (e.g., yield of target cell capture, purity of total cell capture). Given that particle focusing was observed across multiple vertical locations in these experiments, we evaluated inertial focusing quality of in-focus particles at vertical positions $z=58$ (i.e., near the center of the long channel face). Since no accepted metric exists to define inertial focusing quality, we established a non-dimensional term "bandwidth efficiency" $\beta_z$ that is dependent on mean particle diameter $a_m$, the mean lateral distance $z_m$ of an in-focus particle (as an absolute value) from the channel centerline, and the standard deviation $\sigma_z$ of in-focus particles in the z-direction (Table 1). Bandwidth efficiency was defined as $\beta_z = w_b / a_m = (4\sigma_z + a_m) / a_m$, where $w_b$ is the edge-to-edge bandwidth in the z-direction over which 95% of all in-focus particles can be found. Note that $\beta_z$ is normalized by $a_m$, which will vary depending on the class of particles used. As a result, $\beta_z \geq 1$ in all cases, with $\beta_z \sim 1$ when particle focusing is nearly perfect ($\sigma_z \sim 0$). Based on the current imaging and device setup, scanning resolution in the z-direction was comprehensive and continuous, while scanning resolution in the *y*-direction was incomplete and segmented. Nonetheless, we established a non-dimensional term "focusing utility" $\Phi_y$ to serve as a crude measure of particle frequency at vertical positions where predicted particle focusing was unlikely

to occur. Focusing utility $\Phi_y$ was defined as $\Phi_y = n_f/N$, where $n_f$ is the number of in-focus particles at vertical positions $\square=58\square\square$ and $N$ is the number of in-focus particles at vertical positions $\square=18\square\square$. As a result, $\Phi_y \leq 1$ in all cases, with $\Phi_y \sim 1$ when particle focusing is nearly perfect ($n_f \sim N$).

**Inertial focusing behavior of polystyrene beads in blood**

Polystyrene beads have been used extensively to study particle focusing behavior in microchannels.[8,12,14] As ready-to-use monodisperse particles exhibiting strong and uniform fluorescence intensity, polystyrene beads were an ideal choice for this study. Given the mean particle diameter and channel dimensions, the particle Reynolds numbers of polystyrene beads in physiological saline for flow rates $Q$ = 50, 150, and 450 µl/min were $R_p$ = 0.32, 0.97, and 2.91. Using flow rates that correspond to $R_p < 1$, $R_p \sim 1$, and $R_p > 1$, polystyrene beads served as a reference standard for white blood cells and PC-3 cells. For $Q$ = 50 µl/min in physiological saline ($f_{RBC}$ = 0), bead focusing in both the $z$-direction ($\beta_z$ = 1.27) and the $y$-direction ($\Phi_y$ = 0.91) approached optimal levels (Fig. 2) . When $f_{RBC}$ = 0.07, bead focusing decreased moderately in the $y$-direction ($\Phi_y$ = 0.73) with minimal decrease in the $z$-direction ($\beta_z$ = 1.35). When $f_{RBC}$ = 0.33, bead focusing was poorly organized in both the $z$-direction ($\beta_z$ = 2.86) and $y$-direction ($\Phi_y$ = 0.81). For $Q$ = 150 µl/min in physiological saline ($f_{RBC}$ = 0), bead focusing in both the $z$-direction ($\beta_z$ = 1.08) and the $y$-direction ($\Phi_y$ = 1) reached optimal levels. When $f_{RBC}$ = 0.07, bead focusing decreased moderately in the $z$-direction ($\beta_z$ = 1.56) with minimal decrease in the $y$-direction ($\Phi_y$ = 0.96). For $f_{RBC}$ = 0.33, bead focusing decreased further in a similar manner ($\beta_z$ = 1.82, $\Phi_y$ = 0.87) but remained largely intact. For $Q$ = 450 µl/min in physiological saline ($f_{RBC}$ = 0), bead focusing became suboptimal in both the $z$-direction ($\beta_z$ = 1.45) and the $y$-direction ($\Phi_y$ = 0.86), as multiple beads occupied a previously unstable equilibrium position despite a non-unity channel aspect ratio. When $f_{RBC}$ = 0.07, bead focusing decreased minimally in the $z$-direction ($\beta_z$ = 1.54) but improved minimally in the $y$-direction ($\Phi_y$ = 0.91). When $f_{RBC}$ = 0.33, bead

focusing remained largely intact despite a moderate decrease in the *z*-direction ($\beta_z$ = 1.79) and a minimal decrease in the *y*-direction ($\Phi_y$ = 0.86).

**Inertial focusing behavior of white blood cells in blood**

There is significant interest to incorporate inertial focusing into more portable and cost-effective flow cytometry technologies,[2,3] but the focusing behavior (and separation efficiency) of white blood cells (WBCs) in whole or minimally diluted blood has not been studied. Given the mean particle diameter and channel dimensions, the particle Reynolds numbers of WBCs in physiological saline for flow rates $Q$ = 50, 150, and 450 µl/min were $R_p$ = 0.27, 0.80, and 2.41. Since WBCs have a size range of 7-11 µm, the lower bound of $R_p$ = 0.16, 0.48, and 1.46, while the upper bound of $R_p$ = 0.40, 1.20, and 3.60. For $Q$ = 50 µl/min in physiological saline ($f_{RBC}$ = 0), WBC focusing in both the *z*-direction ($\beta_z$ = 1.43) and the *y*-direction ($\Phi_y$ = 0.79) was weaker relative to polystyrene beads (Fig. 3a). In particular, multiple WBCs were found unfocused at vertical positions near the channel floor (i.e., *z*=14 µm). When $f_{RBC}$ = 0.07, WBC focusing decreased moderately in both the *z*-direction ($\beta_z$ = 1.85) and *y*-direction ($\Phi_y$ = 0.55). When $f_{RBC}$ = 0.33, WBC focusing was poorly organized in both the *z*-direction ($\beta_z$ = 3.13) and *y*-direction ($\Phi_y$ = 0.40). For $Q$ = 150 µl/min in physiological saline ($f_{RBC}$ = 0), WBC focusing improved in the *z*-direction ($\beta_z$ = 1.28) but deteriorated in the *y*-direction ($\Phi_y$ = 0.72) as more WBCs were found unfocused at vertical positions near the channel floor. When $f_{RBC}$ = 0.07, particle focusing deteriorated moderately in both the z-direction ($\beta_z$ = 1.82) and the *y*-direction ($\Phi_y$ = 0.61). However, most WBCs were found near a channel wall to the extent that a loose annulus of WBCs appeared to form. When $f_{RBC}$ = 0.33, WBC focusing decreased further in both the *z*-direction ($\beta_z$ = 2.44) and the *y*-direction ($\Phi_y$ = 0.54) as the annulus of WBCs became more radially diffuse. For $Q$ = 450 µl/min in physiological saline ($f_{RBC}$ = 0), WBC focusing decreased moderately the *z*-direction ($\beta_z$ = 1.43) with minimal improvement in the *y*-direction ($\Phi_y$ = 0.75) as WBCs occupying vertical positions near the channel floor became organized around a

previously unstable equilibrium position despite a non-unity aspect ratio. When $f_{RBC}$ = 0.07, WBC focusing decreased moderately in the *z*-direction ($\beta_z$ = 1.82) and reversed in the *y*-direction ($\Phi_y$ = 0.61) as an annulus of WBCs appeared to form. When $f_{RBC}$ = 0.33, WBC focusing decreased moderately in the *z*-direction ($\beta_z$ = 2.33) and minimally in the *y*-direction ($\Phi_y$ = 0.57) as the annulus of WBCs became more radially diffuse. Since the WBCs used were polydisperse in nature, we investigated the relationship between particle diameter *a* and lateral distance $z_f$ of an in-focus WBC (as an absolute value) from the channel centerline (Fig. 3b). Despite the narrow size range observed, larger WBCs were found to be slightly closer to the channel centerline (i.e., smaller $z_f$), while smaller WBCs were primarily accounted for WBCs found unfocused or at vertical positions near the channel floor.

**Inertial focusing behavior of PC-3 cells in blood**

There is significant interest to incorporate inertial focusing into cell-friendly and high-throughput rare cell isolation technologies,[4,5] but the focusing behavior (and separation efficiency) of rare cells such as circulating tumor cells (CTCs) in whole or minimally diluted blood has not been studied. We used a model prostate cancer cell line (PC-3) to assess CTC focusing behavior in blood. Given the mean particle diameter and channel dimensions, the particle Reynolds number of PC-3 cells in physiological saline for the given set of flow rates were $R_p$ = 1.01, 3.04, and 9.11. Since the particle diameter ranged from 10-35 μm, the lower bound of $R_p$ = 0.33, 0.99, and 2.97, while the upper bound of $R_p$ = 3.91, 11.76, and 35.26. For $Q$ = 50 μl/min in physiological saline ($f_{RBC}$ = 0), PC-3 cell focusing in both the *z*-direction ($\beta_z$ = 1.47) and the *y*-direction ($\Phi_y$ = 1) approached optimal levels (Fig. 4a). When $f_{RBC}$ = 0.07, PC-3 cell focusing was largely unaffected in both the *z*-direction ($\beta_z$ = 1.56) and *y*-direction ($\Phi_y$ = 1). When $f_{RBC}$ = 0.33, PC-3 cell focusing decreased moderately in the *y*-direction ($\Phi_y$ = 1) but improved minimally in the *z*-direction ($\beta_z$ = 1.45). Since PC-3 cell focusing remained strong, particularly in the *z*-direction, we repeated this experiment using whole blood ($HCT$ = 45%). For

$f_{RBC}$ = 1, PC-3 cell focusing shifted radically ($\beta_z$ = 1.22, $\Phi_y$ = 0.17) as PC-3 cells were predominantly found along the channel centerline ($z$ = 0) around a previously unstable equilibrium position (due to non-unity channel aspect ratio). No PC-3 cells occupied previously stable equilibrium positions observed at lower $f_{RBC}$. For Q = 150 µl/min in physiological saline ($f_{RBC}$ = 0), PC-3 cell focusing in both the $z$-direction ($\beta_z$ = 1.25) and the $y$-direction ($\Phi_y$ = 1) reached optimal levels. When $f_{RBC}$ = 0.07, PC-3 cell focusing was largely unaffected in both the $z$-direction ($\beta_z$ = 1.32) and $y$-direction ($\Phi_y$ = 1). When $f_{RBC}$ = 0.33, PC-3 cell focusing decreased moderately in both the $z$-direction ($\beta_z$ = 1.45) and the $y$-direction ($\Phi_y$ = 1). For $f_{RBC}$ = 1, PC-3 cell focusing again shifted radically ($\beta_z$ = 1.22, $\Phi_y$ = 0) as PC-3 cells predominantly occupied an equilibrium position (centered on the short face of the channel) not observed at lower $f_{RBC}$. For Q = 450 µl/min in physiological saline ($f_{RBC}$ = 0), PC-3 cell focusing in both the $z$-direction ($\beta_z$ = 1.28) and the $y$-direction ($\Phi_y$ = 1) remained at optimal levels due to the lack of PC-3 cells found at vertical positions near the channel floor (unlike for polystyrene beads and white blood cells). When $f_{RBC}$ = 0.07, PC-3 cell focusing was largely unaffected in both the $z$-direction ($\beta_z$ = 1.28) and $y$-direction ($\Phi_y$ = 1). When $f_{RBC}$ = 0.33, PC-3 cell focusing decreased moderately in both the $z$-direction ($\beta_z$ = 1.35) and the $y$-direction ($\Phi_y$ = 1). When $f_{RBC}$ = 1, PC-3 cell focusing again shifted radically ($\beta_z$ = 1.32, $\Phi_y$ = 0) as described previously for Q = 150 µl/min, but PC-3 cell focusing decreased moderately in the $z$-direction. Since the PC-3 cells used were polydisperse in nature, we investigated the relationship between particle diameter $a$ and lateral distance $z_f$ of an in-focus PC-3 cell (as an absolute value) from the channel centerline (Fig. 4b). When $f_{RBC}$ = 0, 0.07, or 0.33, a linear correlation between the two parameters was observed, where large PC-3 cells were situated closer to the channel centerline ($z$ = 0), while small PC-3 cells were situated closer to the channel wall (z = ± 22.5 µm). When $f_{RBC}$ = 1, large PC-3 cells formed a tighter distribution around the channel centerline relative to small PC-3 cells.

**Rheological properties of test fluids**

In an attempt to gain insight into the radical shift in PC-3 cell focusing behavior when $f_{RBC}$ increased from 0.33 to 1, we used a rotational rheometer with a concentric cylinder geometry to measure the effective viscosity of the test fluid at $f_{RBC}$ = 0, 0.33, and 1 as a function of shear rate (Fig. 5a). The governing equations of motion for a non-Newtonian fluid (such as blood) in a rectangular geometry cannot be reduced to simple equations and solved analytically. However, we used the Power-Law model to describe the test fluid in the *x*-*z* plane for the ideal case of $y$ = 48 μm (i.e., the center of the long channel face) where fluid flow in the *x*-direction can be approximated using a one-dimensional equation. The viscosity $\eta$ of a Power-Law fluid[30] is defined as $\eta = m\left|\gamma'\right|^{n-1}$ where $\gamma'$ is an imposed shear rate, m is a positive constant called the consistency index (with dimensions $Pa \cdot s^n$), and $n$ is a dimensionless positive constant. For a fluid whose viscosity is constant regardless of shear rate (i.e., Newtonian), $n$ = 1. For a fluid whose viscosity decreases with increasing shear rate (i.e., shear-thinning), $n < 1$. Using a log-log plot of viscosity vs. shear rate to calculate $n$, the test fluid was found to be Newtonian ($n$ = 1) for $f_{RBC}$ = 0, very close to Newtonian ($n$ = 0.98) for $f_{RBC}$ = 0.33, and shear-thinning ($n$ = 0.60) for $f_{RBC}$ = 1. Assuming well-developed flow at $y$ = 48 μm, the equation of motion in the *x*-direction can be approximated by $v_x(z) = ((2n+1)/(n+1))\, U_m\, (1 - \left|2z/w\right|^{(n+1)/n})$, where $U_m$ is the mean flow velocity. The shear rate $\gamma'(z) = dv_x(z)/dz$ can also be calculated from this equation. A plot of $v_x(z)$ vs. $z$ (Fig. 5b) and $\gamma'(z)$ vs. $z$ (Fig. 5c) was constructed for $f_{RBC}$ = 0.33 and $f_{RBC}$ = 1. The velocity profile of the test fluid at $f_{RBC}$ = 0.33 was parabolic, while the velocity profile of the test fluid at $f_{RBC}$ = 1 was more blunted. This resulted in a sigmoidal shear rate profile for the test fluid at $f_{RBC}$ = 1 as opposed to a linear shear rate profile for the test fluid at $f_{RBC}$ = 0.33. In particular, there existed a region near the channel centerline ($z$ = 0) where the shear rate of the test fluid at $f_{RBC}$ = 1 was lower (resulting in a higher viscosity) than the shear rate of the test fluid at $f_{RBC}$ = 0.33.

## Discussion

Particle tracking analysis (PTA) was used to identify and characterize individual in-focus particles in diluted and whole blood. Given the brief (~10 ns) yet intense pulses of Nd:YAG laser illumination, individual in-focus particles could be identified (without any visual evidence of fluorescence streak formation) at mean flow velocities up to 1.85 m/s ($Q$ = 450 µl/min), in test fluids up to $HCT$ = 45% ($f_{RBC}$ = 1), and at multiple vertical positions in the microchannel. Direct measurements of these particles were used to generate a two-dimensional ($y$-$z$ plane) profile of particle focusing behavior and its dependence on particle diameter. This represents a significant improvement over what has been achieved using high-speed bright-field imaging and long-exposure fluorescence imaging. In high-speed bright-field imaging, quantitative measurements of individual cell properties can only be made in very dilute ($f_{RBC}$ < 0.07) blood, as the sheer number of RBCs occludes the presence of other cell-sized particles in the channel. In long-exposure fluorescence imaging, a quantifiable intensity curve requires an aggregate fluorescence from a population of particles, which means that particles that are polydisperse in nature cannot be differentiated individually according to size or vertical position.

PTA was first used to observe the inertial focusing behavior of polystyrene beads in diluted blood. Polystyrene beads were chosen as an ideal test case (and reference benchmark) given their monodisperse nature and strong, uniform fluorescence intensity. For particle Reynolds numbers $R_p$ < 1, $R_p$ ~ 1, and $R_p$ > 1 in physiological saline, bead focusing behavior using PTA was largely consistent with previous work in which a microchannel with an original and inverted aspect ratio were used separately to determine the two-dimensional ($y$-$z$ plane) profile of bead focusing behavior.[2] PTA has a significant advantage in providing three-dimensional scanning resolution of particle focusing behavior in a single device over a wide range of $f_{RBC}$, and recent work[31] suggests that PTA image acquisition using a high-speed spinning (Nipkow) disk confocal µPIV system can provide even more comprehensive and

accurate three-dimensional scanning resolution. Assuming that particle focusing behavior is well-developed, images of particles in the *x*-*z* plane can be taken at kHz frequencies in an automated and continuous manner in the *y*-direction with exquisite scanning resolution. PTA image analysis can also be optimized by inputting collected images into a supervised machine learning system such as CellProfiler Analyst[32] for automated recognition of complicated and subtle phenotypes found in millions of particles.

PTA was then used to observe the inertial focusing behavior of white blood cells (WBCs) in diluted blood. Despite the relative similarity in particle diameter between WBCs ($a_m$ = 9.0 μm) and beads ($a_m$ = 9.9 μm), WBC focusing in both the *z*-direction and the *y*-direction was visibly weaker at $f_{RBC}$ = 0. PTA demonstrated the ability to deconstruct WBC focusing behavior based on particle diameter and centroid position of individual particles in the channel cross-section (*y*-*z* plane). As a result, the decrease in WBC focusing behavior (relative to beads) could be partially attributed to smaller WBCs found unfocused at vertical positions near the channel floor. These results are consistent with the notion that small WBCs experience weaker inertial lift forces relative to large WBCs since $R_p \propto a^2$ and are thus more likely to be unfocused at a given $R_p$. PTA also captured the formation of a WBC annulus in the channel cross-section (*y*-*z* plane) at $f_{RBC}$ = 0.07 and 0.33. Leukocyte margination in a straight rectangular channel has been observed at much lower Reynolds numbers but not at the flow rates used in this study.[33,34] *In vitro* experiments characterizing the radial distribution of WBCs have shown that leukocyte margination from the center of a blood vessel depends on rheological factors such as hematocrit, blood suspension medium and shear stress.[35,36] Further investigation into leukocyte margination in inertia-dominated flow will be necessary.

PTA was finally used to observe the inertial focusing behavior of PC-3 cells in diluted blood and whole blood. A model prostate cancer (PC-3) cell line was used as a surrogate for circulating tumor cells (CTCs). CTC isolation poses an immense technical challenge, as CTCs are present in as few as one cell per $10^9$ haematologic cells in the blood of patients with

metastatic cancer.[37,38] At $f_{RBC}$ = 0, PC-3 cell focusing was strong in both the z-direction and the y-direction, and it remained relatively intact at $f_{RBC}$ = 0.07 and $f_{RBC}$ = 0.33. Since PC-3 cells are widely polydisperse in nature ($a$ = 10-35 μm) and can be much larger than polystyrene beads, the inertial lift force on a PC-3 cell is expected to be up to an order of magnitude larger. However, it was unexpected for PTA to not only identify in-focus PC-3 cells at $f_{RBC}$ = 1, but to observe a radical shift in PC-3 cell focusing behavior as opposed to further decreases in both the $z$-direction and the $y$-direction from previously observed equilibrium positions. Despite the increased RBC concentration in the channel at $f_{RBC}$ = 1, the preferred equilibrium position found along the channel centerline near the channel floor made it possible to sufficiently resolve in-focus PC-3 cells. A follow-up experiment (Fig. S2) suggested the existence of an additional equilibrium position that is symmetric in the channel cross-section ($y$-$z$ plane), but it was not possible to sufficiently resolve in-focus particles found at vertical positions near the channel ceiling due to light absorption and scattering of RBCs. The discovery of a novel focusing mode for PC-3 cells in whole blood presents an opportunity to enrich (and ultimately isolate) these cells from cancer patient blood samples at high throughput without the need for near-complete depletion of RBCs from whole blood via RBC lysis buffer or density gradient centrifugation (among other commercially available methods).

In an attempt to provide a physical basis for the radical shift in PC-3 cell focusing behavior at $f_{RBC}$ = 1, rheology measurements of the test fluid were made at $f_{RBC}$ = 0.33 and 1. The test fluid was found to be very close to Newtonian at $f_{RBC}$ = 0.33 and shear-thinning at $f_{RBC}$ = 1. As a result, the flow velocity and shear rate profiles indicated regions of higher viscosity near the channel centerline for the test fluid at $f_{RBC}$ = 1 relative to $f_{RBC}$ = 0.33. This change in viscosity could be attributed to various RBC effects (e.g., packing efficiency, preferred geometry), and labeling of RBCs using long chain dialkylcarbocyanines[39] can be used to track RBCs in the microchannel. However, the concomitant nature of PC-3 cell focusing behavior and blood rheology measurements demonstrates a need for further investigation into the effect

of shear-thinning fluids on PC-3 cell focusing behavior. Given a model shear-thinning fluid with or without RBC-like particles[40], the radical shift in PC-3 cell focusing could be attributed to shear thinning without the particulate nature of natural or synthetic particles, shear thinning with the particulate nature of synthetic particles mimicking RBC behavior, or shear thinning with the particulate nature of RBCs present in whole blood.

## Conclusions

Particle tracking analysis (PTA) was used to identify and characterize the inertial focusing behavior of polystyrene beads, white blood cells, and PC-3 cells in diluted and whole blood. Individual in-focus particles could be identified (without any visual evidence of fluorescence streak formation) at mean flow velocities up to 1.85 m/s ($Q$ = 450 µl/min), in test fluids up to $HCT$ = 45% ($f_{RBC}$ = 1), and at multiple vertical positions in the microchannel. Direct measurements of these particles were used to generate a two-dimensional ($y$-$z$ plane) profile of particle focusing behavior and its dependence on particle diameter. Of particular interest is the ability of PTA to not only identify in-focus PC-3 cells at $f_{RBC}$ = 1, but to observe a radical shift in PC-3 cell focusing behavior as opposed to further decreases in both the $z$-direction and the $y$-direction from previously observed equilibrium positions. PTA can be used to provide an experimental frame of reference for understanding the physical basis of inertial lift forces in whole blood via numerical simulations of particle flow in non-Newtonian fluids at high Reynolds number. PTA can also be used to discover inertial focusing modes that enable particle enrichment (and ultimately isolation) directly from whole blood at high throughput for use in global health diagnostics.

**References**


1 Di Carlo D, *Lab Chip* 2009, **9**, 3038-3046.
2 Hur SC, Tse HTK, Di Carlo D, *Lab Chip* 2010, **10**, 274-280.
3 Oakey J, Applegate RW, Arellano E, Di Carlo D, Graves SW, Toner M, *Anal Chem* 2010, **82**, 3862-3867.
4 Hur SC, Henderson-MacLennan NK, McCabe ERB, Di Carlo D, *Lab Chip* 2011, **11**, 912, 920.
5 Bhagat AAS, Hou HW, Li LD, Lim CT, Han J, *Lab Chip* 2011, **11**, 1870-1878.
6 Wu Z, Willing B, Bjerketorp J, Jansson JK, Hjort K, *Lab Chip* 2009, **9**, 1193-1199.
7 Mao W, Alexeev, *Phys Fluids* 2011, **23**, 051704.
8 Di Carlo D, Irimia D, Tompkins RG, Toner M, *Proc Natl Acad Sci USA* 2007, **104**, 18892-18897.
9 Choi YS, Seo KW, Lee SJ, *Lab Chip* 2011, **11**, 460-465.
10 Chun B, Ladd AJC, *Phys Fluids* 2006, **18**, 031704.
11 Bhagat AAS, Kuntaegowdanahalli, Papautsky I, *Phys Fluids* 2008, **20**, 101702.
12 Di Carlo D, Edd JF, Humphry KJ, Stone HA, Toner M, *Phys Rev Lett* 2009, **102**, 094503.
13 Kim YW, Yoo JY, *J Micromech Microeng* 2008, **18**, 065015.
14 Ho BP, Leal LG, *J Fluid Mech* 1974, **65**, 365-400.
15 Matas J, Morris JF, Guazzelli E, *J Fluid Mech* 2004, **515**, 171-195.
16 Lee W, Amini H, Stone HA, Di Carlo D, *Proc Natl Acad Sci USA* 2010, **107**, 22413-22418.
17 Di Carlo D, Irimia D, Tompkins RG, Toner M, *Proc Natl Acad Sci USA* 2007, **104**, 18892-18897.
18 Fahraeus R, Lindqvist T, *Am J Physiol* 1931, **96**, 562-568.
19 Cokelet GR, Goldsmith HL, *Circ Res* 1991, **68**, 1-17.
20 Long DS, Smith ML, Pries AR, Ley K, Damiano ER, *Proc Natl Acad Sci USA* 2004, **101**, 10060-10065.
21 Goldsmith HL, Marlow JC, *J Colloid Interface Sci* 1979, **71**, 383-407.
22 Lima R, Ishikawa T, Imai Y, Takeda M, Wada S, Yamaguchi T, *J Biomech* 2008, **41**, 2188-2196.
23 Patrick MJ, Chen CY, Frakes DH, Dur O, Pekkan K, *Exp Fluids* 2011, **50**, 887-904.
24 Owens RG, *J Non-Newtonian Fluid Mech* 2006, **140**, 57-70.
25 Fedosov DA, Pan W, Caswell B, Gompper G, Karniadakis GE, *Proc Natl Acad Sci USA* 2011, **108**, 11772-11777.
26 Duffy DC, McDonald JC, Schueller OJA, Whitesides GM, *Anal Chem* 1998, **70**, 4974-4984.
27 Ridler TW, Calvard S, *IEEE T Syst Man Cy* 1978, **8**, 630-632.
28 Meinhart CD, Wereley ST, Gray MHB, *Meas Sci Technol* 2000, **11**, 809-814.
29 Choi YS, Seo KW, Lee SJ, *Lab Chip* 2011, **11**, 460-465.
30 Bird RB, Armstrong RC, Hassager O, *Dynamics of Polymeric Liquids, Vol. 1, Fluid Dynamics* 1987, New York, Wiley (2nd Edition).
31 Klein SA, Posner JD, *Meas Sci Technol* 2010, **21**, 105409.
32 Jones TR, Carpenter AE, Lamprecht MR, Moffat J, Silver SJ, Grenier JK, Castoreno AB, Eggert US, Root DE, Golland P, Sabatini DM, *Proc Natl Acad Sci USA* 2009, **106**, 1826-1831.
33 Jain A, Munn LL, *PLoS ONE* 2009, **4**, e7104.
34 Hou HW, Bhagat AAS, Chong AGL, Mao P, Tan KDW, Han J, Lim CT, *Lab Chip* 2010, **10**, 2605-2613.
35 Schmid-Schonbein GW, Usami S, Shalak R, Chien S, *Microvasc Res* 1980, **19**, 45-70.
36 Goldsmith HL, Spain S, *Microvasc Res* 1984, **27**, 204-222.

37 Krivacic RT, Ladanyi A, Curry DN, Hsieh B, Kuhn P, Bergsrud DE, Kepros JF, Barbera T, Ho MY, Chen LB, Lerner RA, Bruce RH, *Proc Natl Acad Sci USA* 2004, **101**, 10501-10504.
38 Racila E, Euhus D, Weiss AJ, Rao C, McConnell J, Terstappen LW, Uhr JW, *Proc Natl Acad Sci USA* 1998, **95**, 4589-4594.
39 Kamoun WS, Chae S, Lacorre DA, Tyrrell JA, Mitre J, Gillissen M, Fukumura D, Jain RK, Munn LL, *Nature Methods* 2010, **15**, 845-851.
40 Merkel TJ, Jones SW, Herlihy KP, Kersey FR, Shields AR, Napier M, Luft JC, Wu H, Zamboni WC, Wang AZ, Bear JE, Desimone JM, *Proc Natl Acad Sci USA* 2011, 108, 586-591.

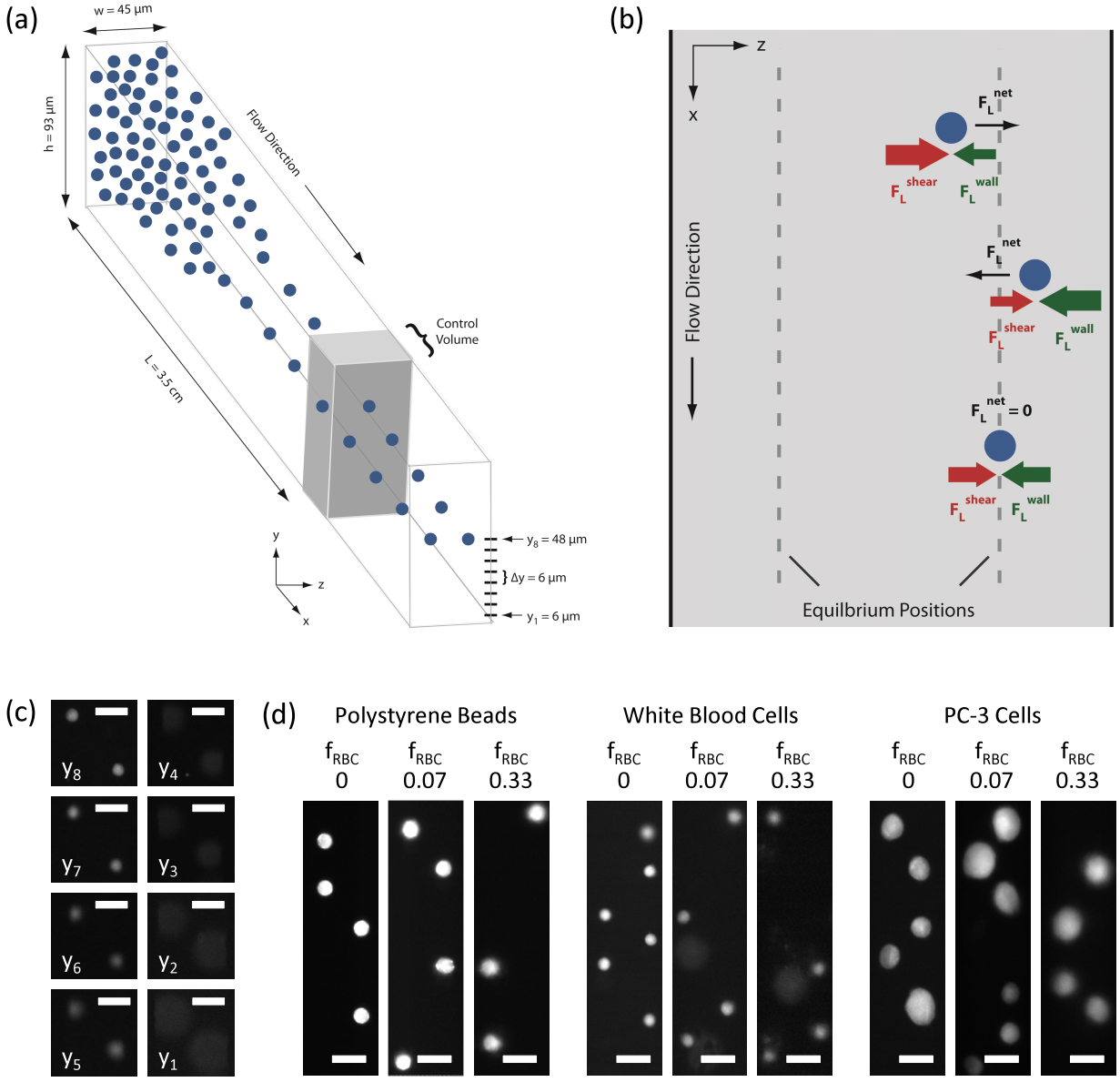


**Fig. 1** Using particle trajectory analysis (PTA) to observe particle focusing behavior in diluted blood. (a) Randomly distributed particles predominantly focus to two lateral positions centered on the long face of a straight microchannel with 2:1 aspect ratio. (b) The equilibrium positions result from a balance of a "wall effect" lift that acts away from the wall towards the channel centerline and a "particle shear" lift that acts away from the channel centerline towards the wall. (c) Particle focusing behavior is observed in the *x*-*z* plane from eight different vertical positions spanning the bottom half of the channel. Focused particles are shown to be in focus at $y_8$ = 48 µm (scale bar = 20 µm). (d) At a flow rate Q = 450 µl/min, PTA images of polystyrene beads ($R_p$ = 2.91 for $f_{RBC}$ = 0), white blood cells ($R_p$ = 2.41 for $f_{RBC}$ = 0) , and PC-3 prostate cancer cells ($R_p$ = 9.11 for $f_{RBC}$ = 0) suspended in physiological saline and diluted blood demonstrate that individual in-focus particles can be identified in starting samples with higher RBC volume fractions ($f_{RBC}$) without significant degradation in fluorescence signal quality.

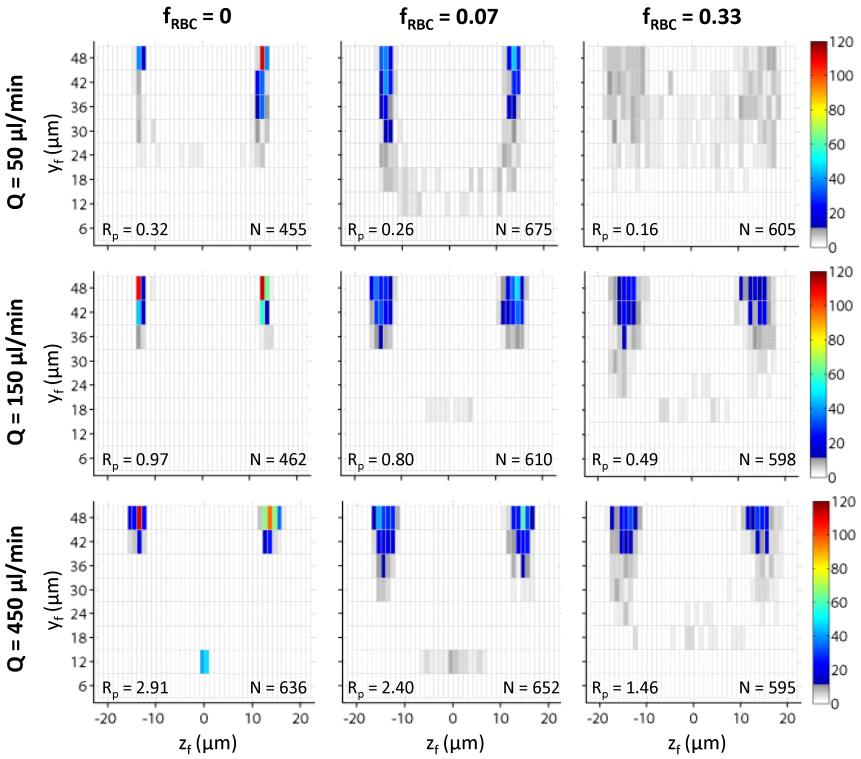


**Fig. 2** Polystyrene bead focusing behavior as a function of flow rate *Q* and RBC volume fraction $f_{RBC}$. For $f_{RBC}$ = 0, values of Q correspond to $R_p$ = 0.32, 0.97, and 2.91. For $f_{RBC}$ = 0.07, values of Q correspond to $R_p$ = 0.26, 0.80, and 2.40. For $f_{RBC}$ = 0.33, values of Q correspond to $R_p$ = 0.16, 0.49, and 1.46. The in-focus vertical position $y_f$ and in-focus lateral distance $z_f$ from the channel centerline for polystyrene beads were used to construct a cross-sectional particle histogram.

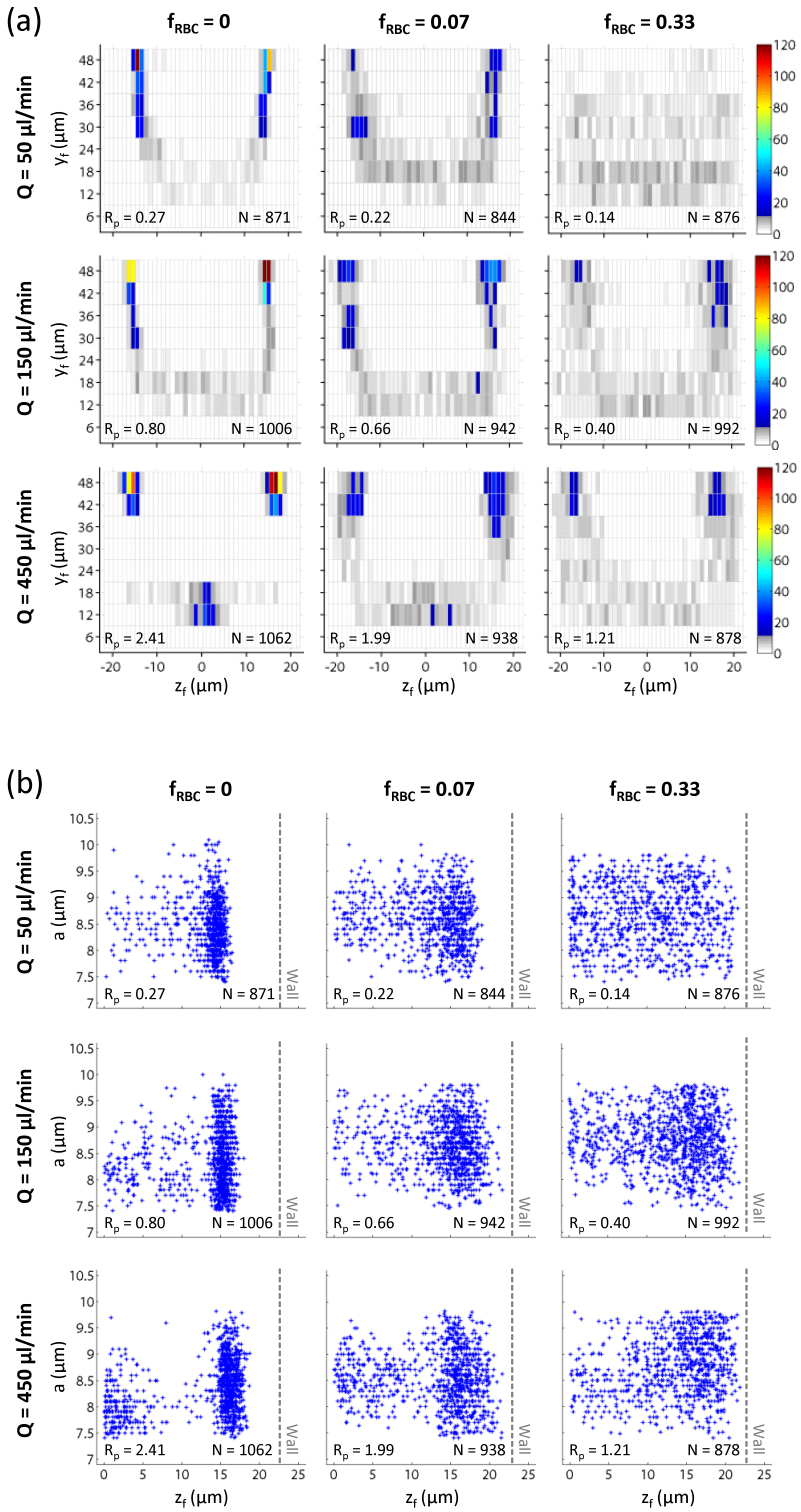


**Fig. 3** White blood cell focusing behavior as a function of flow rate *Q* and RBC volume fraction $f_{RBC}$. For $f_{RBC}$ = 0, values of Q correspond to $R_p$ = 0.27, 0.80, and 2.41. For $f_{RBC}$ = 0.07, values of Q correspond to $R_p$ = 0.22, 0.66, and 1.99. For $f_{RBC}$ = 0.33, values of Q correspond to $R_p$ = 0.14, 0.40, and 1.21. (a) The in-focus vertical position $y_f$ and in-focus lateral distance $z_f$ from the channel centerline for white blood cells were used to construct a cross-sectional particle histogram. (b) The dependence of particle

diameter *a* on in-focus lateral distance $z_f$ was illustrated using a particle scatter plot. The dotted line represents the position at which a given white blood cell would be in contact with the sidewall given a non-deformable microchannel.

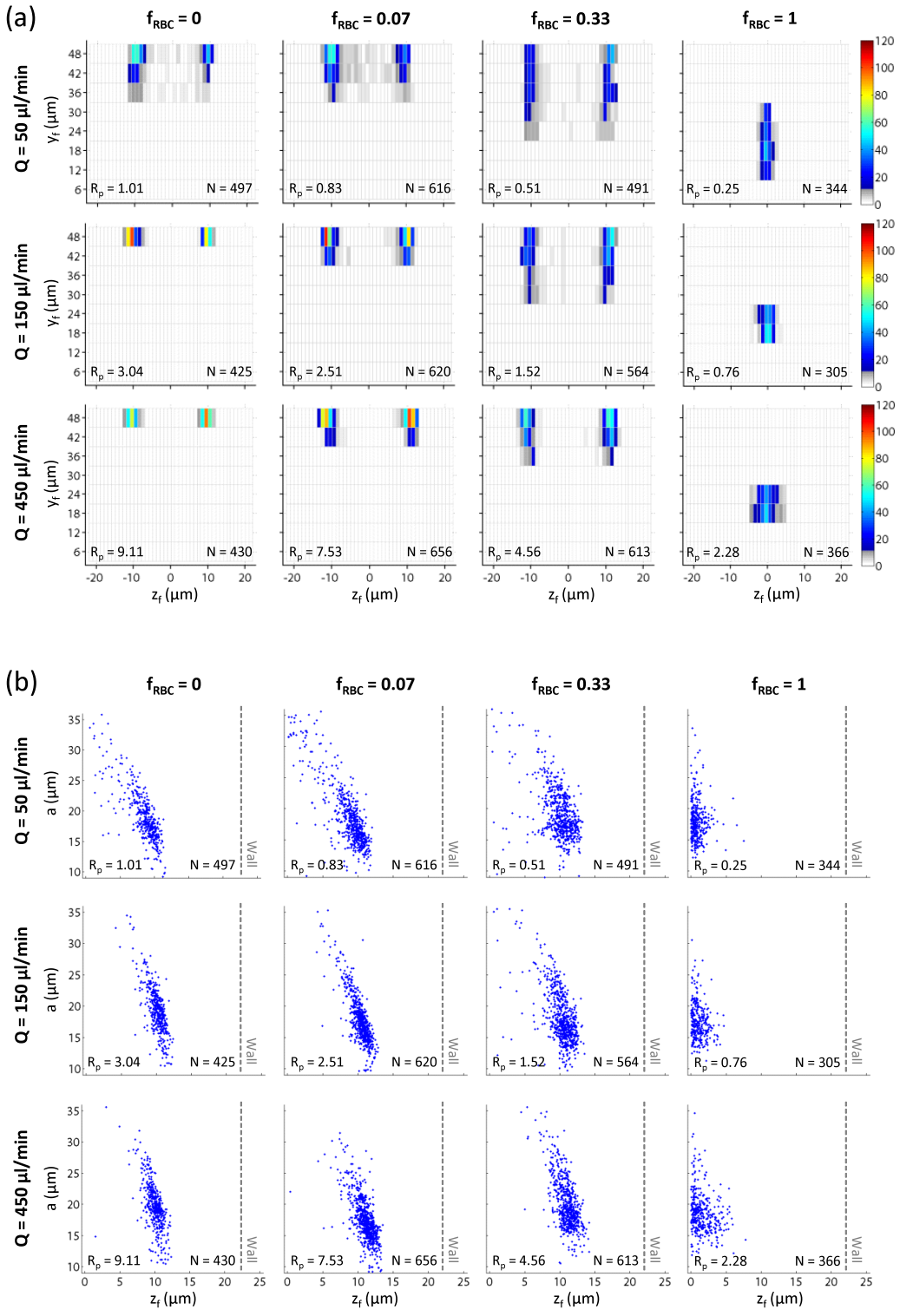


**Fig. 4** PC-3 prostate cancer cell focusing behavior as a function of flow rate *Q* and RBC volume fraction $f_{RBC}$. For $f_{RBC}$ = 0, values of Q correspond to $R_p$ = 0.27, 0.80, and 2.41. For $f_{RBC}$ = 0.07, values of Q correspond to $R_p$ = 0.22, 0.66, and 1.99. For $f_{RBC}$ = 0.33, values of Q correspond to $R_p$ = 0.14, 0.40, and 1.21. (a) The in-focus vertical position $y_f$ and in-focus lateral distance $z_f$ from the

channel centerline for PC-3 cells were used to construct a cross-sectional particle histogram. (b) The dependence of particle diameter *a* on in-focus lateral distance $z_f$ for PC-3 cells was illustrated using a particle scatter plot. The dotted line represents the position at which a given white blood cell would be in contact with the sidewall given a non-deformable microchannel.

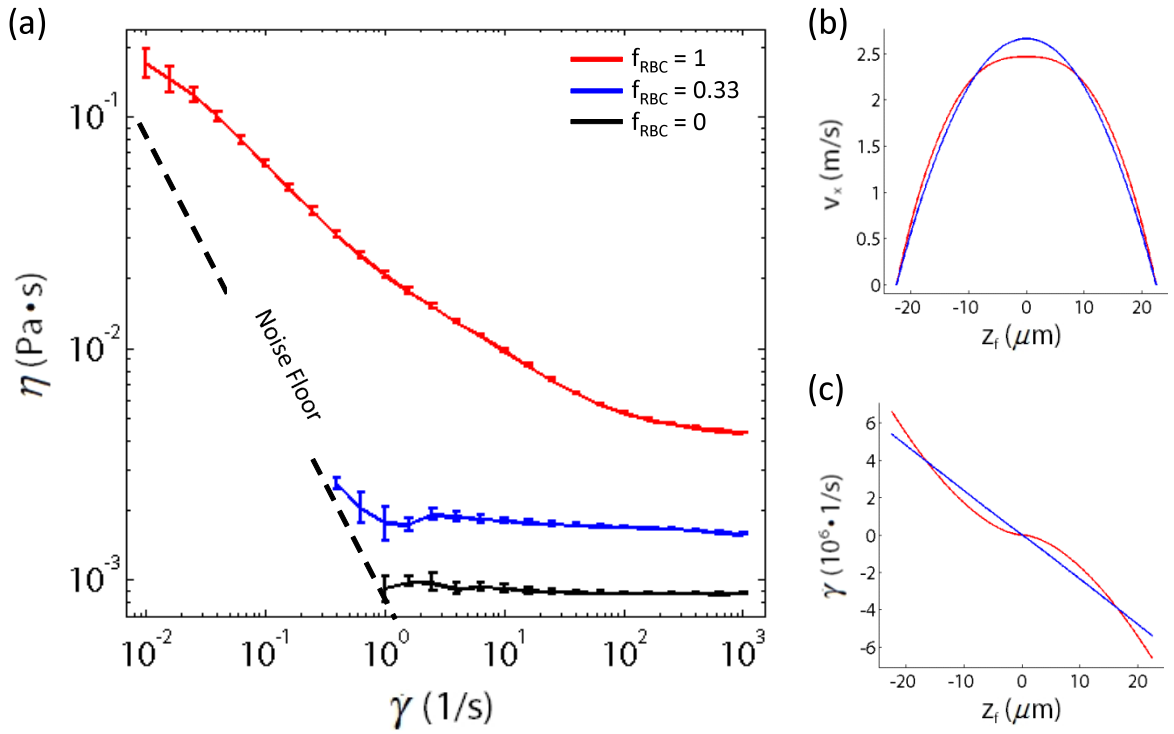


**Fig. 5** Rheometer measurements of diluted and whole blood. (a) The effective viscosity $\eta$ for physiological saline, diluted blood, and whole blood was measured as a function of shear rate $\gamma'$ using a rheometer with a concentric cylinder geometry. (b) Modeling diluted and whole blood as a Power-Law fluid, the flow velocity $v_x$ down the microchannel for diluted and whole blood at height $y$ = 48 μm was calculated as a function of in-focus lateral distance $z_f$ from the channel centerline. (c) Modeling diluted and whole blood as a Power-Law fluid, the shear rate $\gamma'$ for diluted and whole blood at height $y$ = 48 μm was calculated as a function of in-focus lateral distance $z_f$ from the channel centerline.

| | Q (µl/min) | $f_{RBC}$ | $R_p$ | $z_m$ (µm) | $\sigma_z$ (µm) | $\beta_z$ | $\Phi_y$ |
|---|---|---|---|---|---|---|---|
| Polystyrene Beads | 50 | 0 | 0.32 | 12.7 | 0.7 | 1.27 | 0.91 |
| | | 0.07 | 0.28 | 13.5 | 0.9 | 1.35 | 0.73 |
| | | 0.33 | 0.18 | 12.5 | 4.5 | 2.86 | 0.81 |
| | 150 | 0 | 0.97 | 12.9 | 0.5 | 1.08 | 1 |
| | | 0.07 | 0.84 | 14.1 | 1.4 | 1.56 | 0.96 |
| | | 0.33 | 0.56 | 13.9 | 2.1 | 1.82 | 0.87 |
| | 450 | 0 | 2.91 | 13.6 | 1.1 | 1.45 | 0.86 |
| | | 0.07 | 2.53 | 14.2 | 1.4 | 1.54 | 0.91 |
| | | 0.33 | 1.68 | 14.4 | 2.0 | 1.79 | 0.86 |
| White Blood Cells | 50 | 0 | 0.27 | 14.4 | 0.9 | 1.43 | 0.79 |
| | | 0.07 | 0.23 | 15.6 | 2.0 | 1.85 | 0.55 |
| | | 0.33 | 0.16 | 11.2 | 5.3 | 3.13 | 0.40 |
| | 150 | 0 | 0.80 | 15.5 | 0.6 | 1.28 | 0.72 |
| | | 0.07 | 0.70 | 16.5 | 1.9 | 1.82 | 0.61 |
| | | 0.33 | 0.46 | 15.3 | 3.3 | 2.44 | 0.54 |
| | 450 | 0 | 2.41 | 16.1 | 1.0 | 1.43 | 0.75 |
| | | 0.07 | 2.10 | 16.5 | 1.9 | 1.82 | 0.61 |
| | | 0.33 | 1.39 | 16.2 | 2.9 | 2.33 | 0.57 |
| PC-3 Cells | 50 | 0 | 1.01 | 8.6 | 2.1 | 1.47 | 1 |
| | | 0.07 | 0.88 | 8.6 | 2.5 | 1.56 | 1 |
| | | 0.33 | 0.58 | 9.9 | 2.0 | 1.45 | 0.92 |
| | | 1 | 0.25 | 1.0 | 0.9 | 1.22 | 0.17 |
| | 150 | 0 | 3.04 | 10.1 | 1.1 | 1.25 | 1 |
| | | 0.07 | 2.64 | 10.3 | 1.4 | 1.32 | 1 |
| | | 0.33 | 1.76 | 10.2 | 1.8 | 1.41 | 1 |
| | | 1 | 0.76 | 1.1 | 1.0 | 1.22 | 0 |
| | 450 | 0 | 9.11 | 9.9 | 1.2 | 1.28 | 1 |
| | | 0.07 | 7.92 | 11.0 | 1.3 | 1.28 | 1 |
| | | 0.33 | 5.27 | 10.8 | 1.5 | 1.35 | 1 |
| | | 1 | 2.28 | 1.7 | 1.4 | 1.32 | 0 |

**Table 1** Quantitative measurements of particle focusing behavior as a function of flow rate $Q$ and RBC volume fraction $f_{RBC}$. For a given $Q$ and $f_{RBC}$, the particle Reynolds number $R_p$, the mean in-focus lateral distance $z_m$ from the channel centerline, the bandwidth efficiency $\beta_z$ ,and the focusing utility $\Phi_y$ were calculated for polystyrene beads, white blood cells, and PC-3 prostate cancer cells.

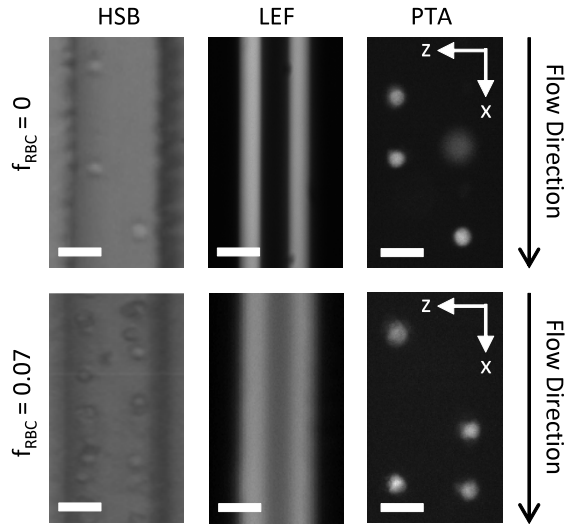


**Fig. S1** Imaging techniques used to study particle focusing in a microchannel. All images were taken at a vertical position $y$ = 45 μm. For high-speed bright-field (HSB) microscopy with an exposure time of 2 μs, individual white blood cells can be identified in physiological saline ($f_{RBC}$ = 0) but not in diluted blood ($f_{RBC}$ = 0.07). For long-exposure fluorescence (LEF) microscopy with an exposure time of 1 s, a bulk white blood cell distribution profile can be identified, but the profile cannot be de-constructed based on height position or particle diameter. For particle tracking analysis (PTA) with an exposure time of 10 ns, individual white blood cells re-suspended in physiological saline or diluted blood can be identified at multiple vertical positions in the channel (scale bar = 20 μm).

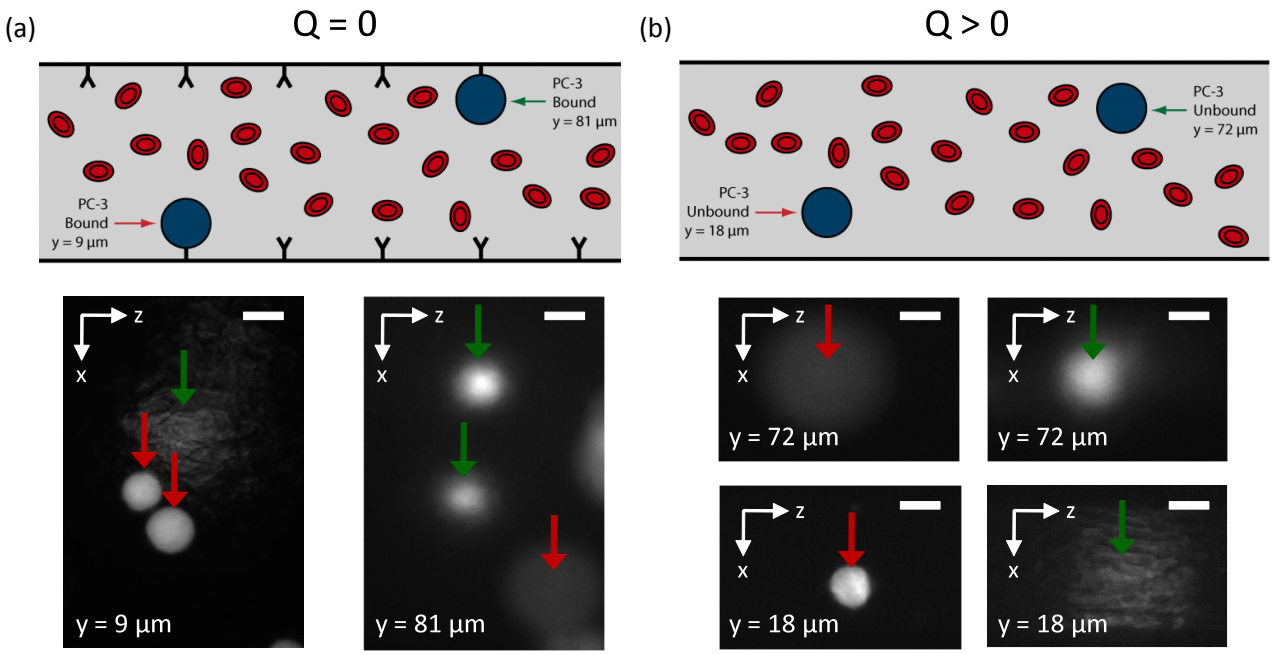


**Fig. S2** Identifying PC-3 cells re-suspended in whole blood ($f_{RBC}$ = 1, *HCT* = 45%). (a) A straight rectangular channel with 2:1 aspect ratio was functionalized with anti-EpCAM antibody, which binds to EpCAM surface markers found on PC-3 cells. After PC-3 cells were captured in the channel, images were taken near the channel floor ($y$ = 9 µm) to visualize PC-3 cells attached to the channel floor (red arrow) and the channel ceiling (green arrow). Images were also taken near the channel ceiling ($y$ = 81 µm) to visualize PC-3 cells attached to the channel floor (red arrow) and the channel ceiling (green arrow). (b) In an unfunctionalized channel, images were taken at $y$ = 18 µm to visualize PC-3 cells flowing near the channel floor (red arrow) and the channel ceiling (green arrow). Images were also taken at $y$ = 72 µm to visualize PC-3 cells flowing near the channel floor (red arrow) and the channel ceiling (green arrow).